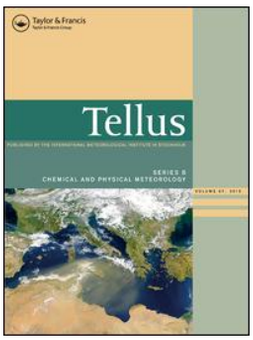

Tellus B: Chemical and Physical Meteorology

ISSN: (Print) 1600-0889 (Online) Journal homepage: http://www.tandfonline.com/loi/zelb20

Arctic haze over Central Europe

Jost Heintzenberg, Thomas Tuch, Birgit Wehner, Alfred Wiedensohler, Heike Wex, Albert Ansmann, Ina Mattis, Detlef Müller, Manfred Wendisch, Sabine Eckhardt & Andreas Stohl

To cite this article: Jost Heintzenberg, Thomas Tuch, Birgit Wehner, Alfred Wiedensohler, Heike Wex, Albert Ansmann, Ina Mattis, Detlef Müller, Manfred Wendisch, Sabine Eckhardt & Andreas Stohl (2011) Arctic haze over Central Europe, Tellus B: Chemical and Physical Meteorology, 55:3, 796-807, DOI: 10.3402/tellusb.v55i3.16366

To link to this article: https://doi.org/10.3402/tellusb.v55i3.16366

Published online: 15 Dec 2016.

Tellus (2003), 55B, 796–807
Printed in UK. All rights reserved

TELLUS
ISSN 0280–6509

Arctic haze over Central Europe

By JOST HEINTZENBERG[1]*, THOMAS TUCH[1], BIRGIT WEHNER[1], ALFRED WIEDENSOHLER[1], HEIKE WEX, ALBERT ANSMANN[1], INA MATTIS[1], DETLEF MÜLLER[1], MANFRED WENDISCH[1], SABINE ECKHARDT[2] and ANDREAS STOHL[2], [1]*Leibniz-Institute for Tropospheric Research, Permoserstrasse 15, 04318 Leipzig, Germany;* [2]*Department of Ecology, Technical University Munich, Am Hochanger 13, 5354 Freising-Weihenstephan, Germany*

(Manuscript received 9 September 2002; in final form 11 December 2002)

ABSTRACT

An extraordinary aerosol situation over Leipzig, Germany in April 2002 was investigated with a comprehensive set of ground-based volumetric and columnar aerosol data, combined with aerosol profiles from lidar, meteorological data from radiosondes and air mass trajectory calculations. Air masses were identified to stem from the Arctic, partly influenced by the greater Moscow region. An evaluation of ground-based measurements of aerosol size distributions during these periods showed that the number concentrations below about 70 nm in diameter were below respective long-term average data, while number, surface and volume concentrations of the particles larger than about 70 nm in diameter were higher than the long-term averages. The lidar aerosol profiles showed that the imported aerosol particles were present up to about 3 km altitude. The particle optical depth was up to 0.45 at 550 nm wavelength. With a one-dimensional spectral radiative transfer model top of the atmosphere (TOA) radiative forcing of the aerosol layer was estimated for a period with detailed vertical information. Solar aerosol radiative forcing values between -23 and -38 W m^{-2} were calculated, which are comparable to values that have been reported in heavily polluted continental plumes outside the respective source regions. The present report adds weight to previous findings of aerosol import to Europe, pointing to the need for attributing the three-dimensional aerosol burden to natural and anthropogenic sources as well as to aerosol imports from adjacent or distant source regions. In the present case, the transport situation is further complicated by forward trajectories, indicating that some of the observed Arctic haze may have originated in Central Europe. This aerosol was transported to the European Arctic before being re-imported in the modified and augmented form to its initial source region.

1. Introduction

The traditional European classification of polar continental air masses calls for cold and dry air with high visibilities, which in the case of marine air flow should be extremely high, often approaching Rayleigh limits in terms of light scattering. However, beginning with the Arctic Ptarmigan flights of the 1950s (Mitchell, 1959) and increasingly after the realization of the Arctic haze phenomenon in the 1970s (Rahn et al., 1977; Shaw, 1975), high winter and springtime aerosol burdens were found over all of the Arctic.

Through source-receptor studies, (e.g., Rahn, 1982) and trajectory analyses, (e.g., Heintzenberg and Larssen, 1983), these aerosols were identified to originate mostly from Eurasian sources. The particle size distribution of the Arctic haze aerosol clearly indicated that it was dominated by aged particles from which coagulation and dry deposition processes had removed most of the particles with diameters below 50 nm and above 1000 nm after 20 d of atmospheric residence (Heintzenberg et al., 1986). Figure 2 in Covert and Heintzenberg (1993) may serve as a typical example of the monomodal particle number size distribution of Arctic haze.

Over Central Europe, such monomodal number size distributions have not been reported for boundary layer

*Corresponding author.
e-mail: jost@tropos.de

aerosols based on state-of-the-art particle sizing instruments. Instead, three to four modes have been found consistently in the submicrometre particle size range (Birmili et al., 2001) near Leipzig, Germany.

During the first half of April 2002, however, particle number size distributions deviated significantly from the typical multimodal pattern in Leipzig. The measurements were conducted with identical instrumentation as utilized for the long-term statistical study of Birmili et al. (2001). At times, the shape of the measured particle number size distributions was quite similar to that typical of Arctic haze. Air mass back trajectories indicated their Arctic origin. The average distance from the Arctic circle on these trajectories was some 3000 km, which was covered in about 6 d, suggesting the possibility of Arctic aerosols being readvected back to Central Europe.

In order to understand this highly untypical aerosol development a systematic study was conducted. This investigation comprised a comprehensive and unique synopsis and combination of ground-based particle number size distributions and sun photometer data, vertical lidar profiles, radiosondes, back trajectories and tracer transport modeling. The radiative effect of this unusual aerosol was quantified with a detailed radiative transfer model.

2. Methods

2.1. Volumetric measurements

Dry submicrometre number size distributions of aerosol particles are measured continuously at the Institute for Tropospheric Research (IfT) in Leipzig, Germany with electrical-mobility size spectrometers, which classify charged particles, based on their electrical mobility, which is proportional to particle size. The relative humidity in the electrical mobility spectrometers was below 5%. An electrical mobility spectrometer consists of a bipolar aerosol charger, a differential mobility analyzer (DMA) and a condensation particle counter (CPC). In the bipolar charger, the aerosol is brought into bipolar charge equilibrium. The charged particles are segregated in the DMA into different mobility classes, which are equivalent to different particle sizes. The number concentration of particles in different mobility classes in DMAs are counted by a CPC, and the number concentration and size distribution are calculated using a data inversion routine that includes the bipolar charge distribution (Wiedensohler, 1988), the transfer function of the DMA (Birmili et al., 1997), and the counting efficiency of the CPC (Wiedensohler et al., 1997).

The particle diameter range from 3 to 800 nm was covered by operating two DMAs in parallel downstream of a PM10-inlet (50% cut size at 10 μm) on the roof of IfT. This twin differential mobility particle sizer (TDMPS) is a combination of two DMAs in conjunction with two CPCs. The TDMPS system is based on the design of Birmili et al. (1999), with the first DMPS measuring particles from 3–20 nm and the second DMPS measuring particles from 20–800 nm. The TDMPS system uses automated flow controllers, which allows accurate, long-term and unattended measurements.

Volumetric scattering coefficients were measured continuously with an integrating nephelometer (TSI 3563, TSI Minneapolis, MN) with a time resolution of 1 min. The values for the wavelength 550 nm were averaged over the lidar measuring periods given in Table 1.

2.2. Lidar

A multi-wavelength aerosol Raman lidar (Mattis et al., 2002a) at IfT was used to characterize the vertical distribution of the particles in terms of the spectral volume backscatter coefficient (BC) at 355, 532 and 1064 nm wavelength and the spectral extinction coefficients (EC) at 355 and 532 nm, as well as in terms of microphysical properties (Müller et al., 2001). The lidar is part of the European Aerosol Research Lidar Network (EARLINET, Bösenberg et al., 2000). EARLINET observations are routinely performed on Mondays (early afternoon and early evening after sunset) and Thursdays (after sunset). Each observation typically lasts 1 h. Because of favorable weather conditions, lidar observations were possible on every Monday and Thursday of the first half of April 2002. The lidar was running continuously on 8–9 April 2002 for 24 h starting at 1400 UTC (1600 local time) because of the almost cloudless conditions on both days.

2.3. Sun photometer and meteorological data

A CIMEL sun photometer (CIMEL Electronique, Paris, France) automatically and autonomously measured the particle optical depth at six wavelengths between 340 and 1020 nm in the framework of the Aerosol Robotic Network (AERONET, Holben et al., 1998) on the roof of the IfT whenever atmospheric conditions allowed. Several Vaisala-RS80-A radiosondes were launched for sounding of temperature,

pressure and relative-humidity profiles during the intensive measurement period with continuous lidar measurements on 8–9 April 2002.

2.4. Trajectories

To relate the enhanced particle concentrations to possible source regions, arrays of three-dimensional 10-d back trajectories were calculated ending at IfT (with a vertical resolution of 0.25 km up to 10 km above sea level) every 3 h for the first half of April. The trajectory model FLEXTRA version 3.5 (Stohl et al., 1995; Stohl and Seibert, 1998) was used with global meteorological input fields from the European Center for Medium-Range Weather Forecasts (ECMWF, 1995). The horizontal resolution is 1° for all 60 vertical model levels. The time resolution is 3 h (analyses at 0, 6, 12, 18 UTC; 3-h forecasts at 3, 9, 15, 21 UTC). Bicubic interpolation in the horizontal, quadratic interpolation in the vertical and linear interpolation in time were used to interpolate data from the model grid points to the actual trajectory positions. North of 75°N, a polar stereographic projection is applied in order to increase the accuracy of interpolation at high latitudes and to avoid a singularity at the pole.

2.5. Dispersion modeling

The Lagrangian particle dispersion model FLEXPART version 4.4 (for a recent application see e.g., Stohl et al., 1998; 2002), driven with the meteorological analyses from ECMWF, was used to calculate the transport of three anthropogenic emission tracers. Emissions from (a) within the Arctic circle, (b) the greater Moscow region (36–39°E, 55.4– 56.4°N) and (c) European emissions (excluding the former two regions) were differentiated. As a proxy for anthropogenic emissions, carbon monoxide emissions from the EDGAR version 3.2 inventory were used, which is valid for the base year 1995 (Olivier and Berdowski, 2001). Assuming temporally constant emission rates, FLEXPART simulated the atmospheric transport of the emissions occurring from 16 March until 16 April by following the trajectories of 10^6 particles, each carrying the same mass and flagged with its source region, that were released in accordance with the emission distribution. Movies of the horizontal tracer distribution as well as time series of the concentrations obtained for the Leipzig site were used to study the relation of these tracers to the measurements at Leipzig.

2.6. Radiative transfer modeling

For the radiative transfer calculations, a detailed spectral model was utilized (Wendisch et al., 2002). The code calculates vertical profiles of up- and down-welling spectral irradiances, from which the broadband-solar irradiances are obtained by spectral integration. The radiative forcing of the particles was derived as the difference of the upwelling irradiances at the top of the atmosphere calculated without and with aerosol particles. The radio soundings were used for the meteorological model input. Aerosol particles are explicitly treated by their size distribution and subsequent Mie calculations to derive profiles of their spectral volume extinction coefficient, single scattering albedo and phase function. The humidity growth of the particles was considered using the growth factors for ammonium sulfate by Tang and Munkelwitz (1993). The ground-based TDMPS number size distributions were converted to volume size distributions and fitted to a lognormal type of function, which is characterized by three parameters: total particle volume concentration, standard deviation and average diameter. The vertical profile of the particle size distribution was reconstructed using the relative profile data of the particle backscattering coefficient from the lidar measurements and the ground-based particle size distribution measurements (TDMPS). The relative lidar profile was scaled at the ground with the total particle volume concentration from the TDMPS. This ground-based value was then extrapolated into the vertical direction using the relative lidar profile, whereas the standard deviation and the average diameter of the lognormal distribution were fixed. The consistency of the particle model input constructed in that way was tested once in the center of the haze period by calculating the spectral columnar particle optical thickness from the microphysical model input and comparing it with the independent sun photometer measurements. This comparison yielded very good agreement. The root mean square error between the measured and calculated spectral particle optical thickness was 1.7% for the spectral range covered by the sun photometer.

3. Results and discussion

3.1. Trajectory analysis

The interpretation of the measurements was guided by the trajectory-based air mass information.

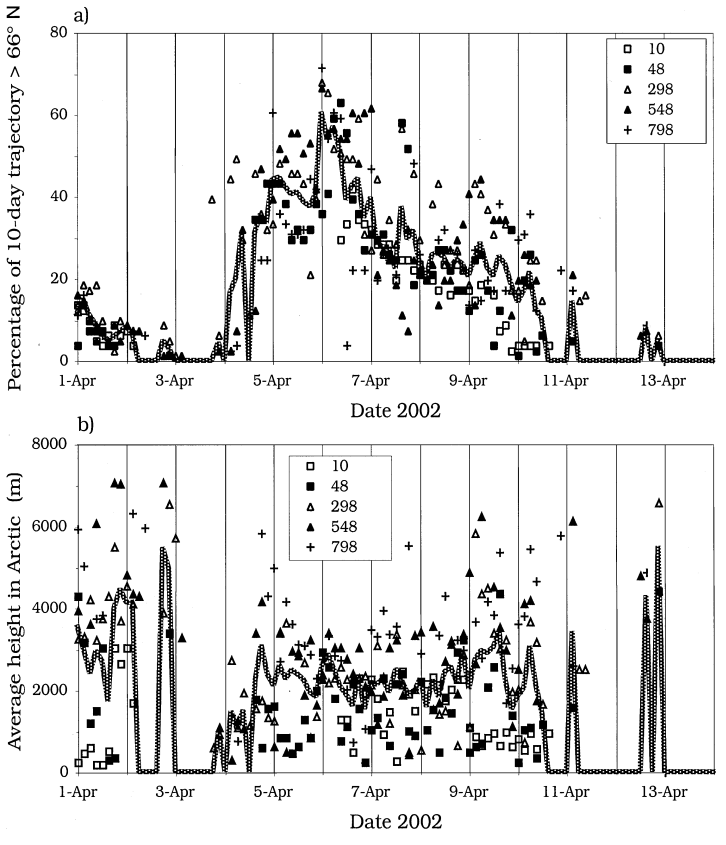

Fig. 1. (a) Individual and average percentage of 10-d trajectory length that trajectories arriving over Leipzig, Germany at the heights 10, 48, 298, 548 and 798 m asl have spent north of 66° latitude during the time period 1–15 April 2002; (b) as (a) but for heights (in m) spent north of 66° latitude.

Using a statistical analysis of trajectories arriving over Leipzig in five height intervals between the surface and 1000 m, the percentage time (of their 10-d length in total) during which the air mass was over the Arctic circle was calculated. This quantity is called the Arctic percentage trajectory time in the following text. For the period 1–13 April this information is summarized in Fig. 1a. The heights (in m) in which the respective trajectories passed over the Arctic are plotted in Fig. 1b. Whereas the individual Arctic percentage trajectory times scatter between a few and more than 70%, average percentage times show contiguous periods with Arctic percentage trajectory times significantly larger than zero between 4 and 10 April. Figure 1b shows that during this period many of the Arctic trajectories remained well below 3000 m during their stay in the Arctic. On average most of the Arctic trajectories were below about 2000 m, many of these close to the surface. This finding is an indication that Arctic surface air indeed affected the investigated air mass. Thus for the period 4–10 April, a more detailed data evaluation was conducted.

The geographical coverage of the Arctic trajectories can be gleaned from Fig. 2, which shows the coordinates of the arithmetic average trajectory for the contiguous period, in which at least 1% (on average 25%) of trajectory length reached beyond the Arctic circle (4 April 2002, 03:00 UTC–10 April 2002, 15:00 UTC). For each trajectory time step, standard deviations of the coordinate positions were calculated and displayed separately as longitude and latitude variability ranges in Fig. 2. A very broad area reaching from 10 to 130°E is covered by the Arctic parts of the back trajectories.

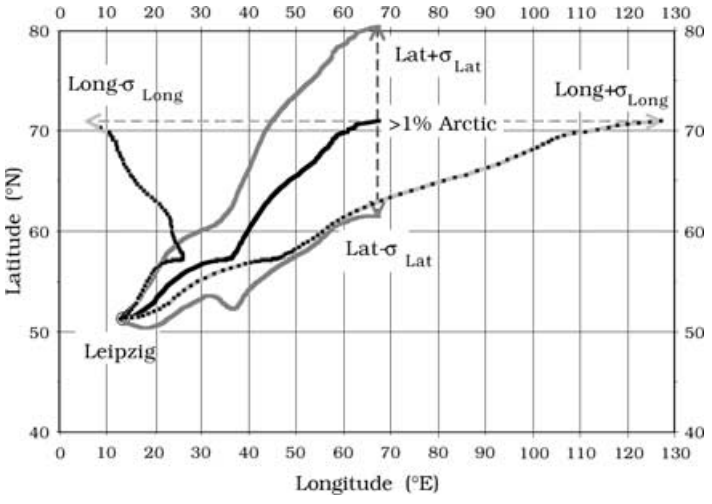

Fig. 2. Arithmetic average 10-d back trajectory for the contiguous period 4 April 2002, 03:00 UTC to 10 April 2002, 15:00 UTC (bold line). The line Lat $\pm\sigma_{\mathrm{Lat}}$ delineates $\pm$ one standard deviation in latitude about the average trajectory. The line Long $\pm\sigma_{\mathrm{Long}}$ delineates $\pm$ one standard deviation in longitude about the average trajectory. The positions $\pm\sigma_{\mathrm{Lat}}$ and $\pm\sigma_{\mathrm{Long}}$ through the starting point of the average trajectory are connected with dashed arrows, respectively. The receptor site is marked by an encircled cross.

3.2. Dispersion modeling

More insight into the sources of the aerosol over Leipzig than from trajectories can be obtained from the CO aerosol proxy. Figure 3 gives the calculated time series of ground-based CO concentrations over Leipzig resulting from Arctic, Moscow and European emissions after 16 March 00:00 UTC, plotted from 1–13 April. Below a stable background of European contributions, a broad period with contributions from Arctic emissions is distinguished, with an absolute peak of the Arctic contributions on 6 April. Contributions from the Moscow region show two peaks reaching up to 10% of the corresponding European contributions. Incidentally, Moscow contributions were reduced to less than 10% of their peak values during the period with maximum Arctic contributions (cf. Fig. 3).

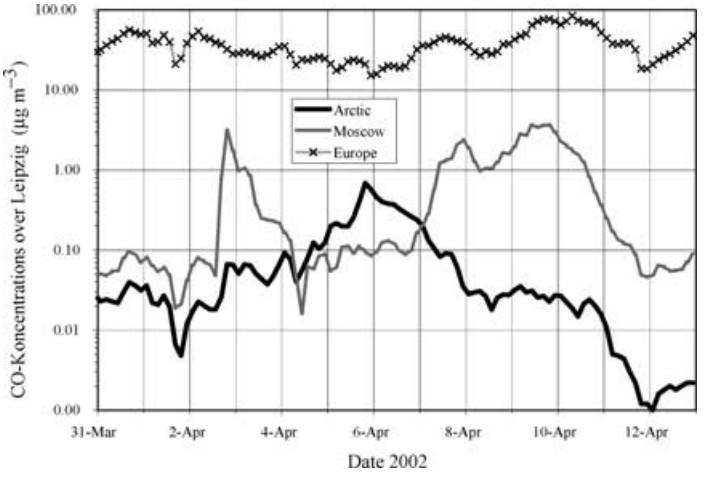

Fig. 3. Time series of calculated CO concentrations over Leipzig from Arctic (>66° latitude), Moscow (delineated by 36–39° longitude, 55.4–56.4° latitude), and European emissions (excluding the former two regions).

3.3. Particle size distributions

Similarly to the CO tracer calculations, the in situ particle size distribution data were classified according to their origin as quantified by the trajectory information. Average number, surface and volume concentration size distributions are presented in Figs. 4a–c. For the surface and volume distributions, spherical particle shape was assumed. These distributions are compared to long-term average data taken with the same instrumentation at Leipzig over the first half of all April months from 1997 to 2001. As a measure of the scatter of the long-term data, average values plus one standard deviation were also plotted in Figs. 4a–c. Of the 2002 data, averages were formed for contiguous periods with at least 1% and at least 1/3 of trajectory lengths in the Arctic. Average Arctic trajectory percentages were 25 and 45%, respectively, in these periods. The latter period reached from 4 April 2002 18:00 UTC to 7 April 2002 00:00 UTC. For a contiguous 9 h in which trajectories passed over the greater Moscow emission region, separate averages were calculated.

The IfT site is located in the eastern outskirts of the city of Leipzig (≈470 000 inhabitants). Consequently, local emissions, in particular traffic- and to some extent heating-related, may influence the aerosol data. Because of the focus on northeasterly wind conditions in the present study, this influence is minimized, yet cannot be excluded completely. In particular, during the second half of the day, local influence was less pronounced and size distributions with high particulate volume concentrations and low ultrafine (<20 nm) number concentrations were recorded. In order to filter out periods with long-range dominance, the additional constraint of number-median diameters (DgN) of at least 70 nm was formulated. This condition is related to the fact that below about 80 nm all number concentrations in April 2002 were lower than the long-term average. On the other hand, above that size excess number, surface and volume concentrations were recorded frequently during the present study.

Number size distributions for the two Arctic trajectory classes (>1% and >33% trajectory length in the Arctic) are characterized by a small Aitken mode (20–80 nm), the occurrence of an ultrafine mode and a relatively large accumulation mode (>80 nm). Many more recently nucleated ultrafine particles were found in the "Moscow air mass." At the same time, this group exhibited very high accumulation mode number fractions, which were only surpassed at sizes beyond 150 nm in the sub-group DgN ≥ 70 nm. The shape of the number distribution in the latter sub-group strongly resembles that reported in Arctic haze for March/April 1989 over Spitsbergen (cf. Fig. 2 in Covert and Heintzenberg, 1993), albeit with twenty times higher total numbers in April 2002 over Leipzig.

Both surface and volume concentration size distributions are monomodal, with a high excess above the corresponding long-term averages for all sizes above about 80 nm. Only beyond 400 nm particle size do long-term averages plus one standard deviation surpass the April 2002 surface and volume concentrations. The relative magnitudes of surface and volume distributions of the different sub-group averages are different compared to the case of particle number concentration. Highest surface and volume concentrations are found for the ≥1% Arctic + DgN ≥ 70 nm sub-group, even higher than in "Moscow air masses." Only beyond about 350 nm do the long-term average surface and volume surpass the corresponding values in the sub-group with lowest concentrations (≥40% Arctic).

3.4. Sun photometer data

Average aerosol optical depths (±1 standard deviation) over Leipzig were calculated for the 1% and 33% Arctic period. For 532 nm wavelength the values were 0.25 ± 0.13 and 0.30 ± 0.13, respectively. On individual days during these periods, considerably higher optical depths were recorded (cf. Table 1). In particular, the "33% Arctic" value is high compared to long-term averages for April at the nearest sun photometer station of the German Weather Service at Lindenberg. For all April months in the period 1997–2001, average optical thicknesses at 550 nm wavelength were 0.20, with a standard deviation of 0.11. We note also that average daytime boundary layer relative humidities were with ≤ 60% below long-term averages.

3.5. Lidar results

A time–height display of the 1064-nm lidar backscatter signal in Fig. 5 gives the temporal development of the haze layer during the period from 8 April, 14:02 UTC (16:02 local time), to 9 April, 14:12 U. The 1064 nm backscatter signal is rather sensitive to any aerosol layer in the troposphere. Different timescales characterize the development of the boundary layer (diurnal cycle) and the Arctic pollution layer.

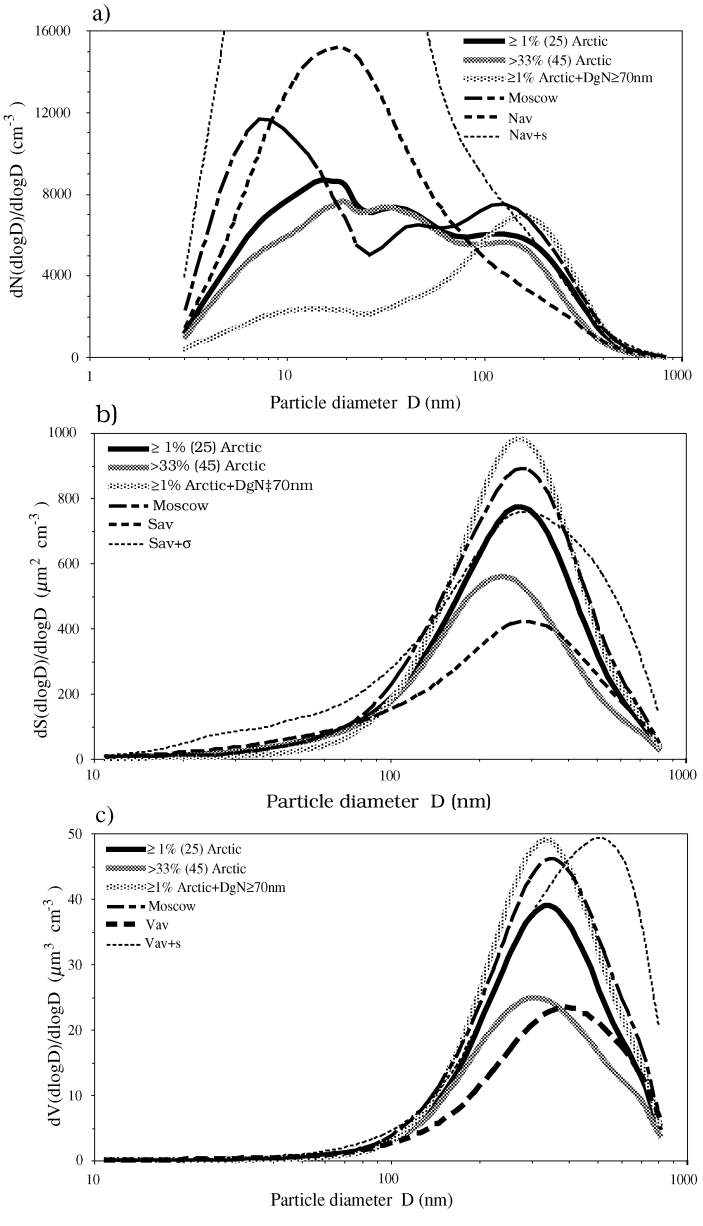

Fig. 4. (a) Trajectory-classified number size distributions at IfT, Leipzig during the period 1–15 April 2002 averaged over the contiguous period with at least 1% of trajectory length in the Arctic (average length 25%) are plotted as a bold line ≥1% (25) Arctic. Corresponding averages over the contiguous period with at least 1/3 of trajectory length in the Arctic (average length 45%) are plotted as the strongly stippled line ≥33% (45) Arctic. Corresponding averages over the contiguous period with at least 1% of trajectory length in the Arctic but also exhibiting number median diameters ≥70 nm are plotted as the lightly stippled line ≥33% (45) Arctic. Average number size distributions at IfT, Leipzig during the period 1–15 April 2002 for trajectories having passed over the greater Moscow area are shown as the bold short/long-dashed line Moscow. Long-term average data for the period 1–15 April during the years 1997–2001 are displayed as the bold dashed line Nav. Long-term averages plus one standard deviation are shown as the thin dashed line Nav + σ. (b) is organized as (a) but for surface size distributions. (c) is organized as (a) but for volume size distributions.

Table 1. *Comparison of characteristic aerosol parameters from ground-based data (TDMPS, nephelometer, sun photometer) and lidar inversions on 8 April 2002, 18:23–19:22 UTC*

Parameter	Ground-based	Lidar
Total surface concentration, $\mu m^2\ cm^{-3}$	630	540[f]
Total volume concentration, $\mu m^3\ cm^{-3}$	29	21[f]
Effective particle diameter, μm	0.28	0.24[f]
Volumetric scattering coefficient, $M\ m^{-1}$	120[a]	170–220[b,f]
Aerosol Optical Depth AOD at 532 nm	0.44[c,d]	0.4[g]
Ångström exponent, *å*	1.8[c,d]	1.7–2[e]

Footnotes add details of the individual measurements:
[a]550 nm.
[b]532 nm.
[c]Average 12–17 UTC.
[d]440–670 nm.
[e]355–532 nm.
[f]Height range 1800–2000 m.
[g]AOD, backscatter coefficient BC (532 nm).
[h]LR, assuming a lidar ratio LR of 50 sr.

The wavelike structure below 2.5 km height indicates the boundary layer. Above the boundary layer the top height of the Arctic haze layer (light gray) descends with time from 3 km to about 2.5 km height. White spots in the upper part of the boundary layer indicate fair-weather cumulus clouds. Aerosol structures above 3.5 km height result from particles probably advected from North America.

Contiguous backscatter structures over several hours were also observed in the free troposphere above 4 km height. In Fig. 6 backward trajectories arriving at Leipzig at 400, 1400 and 2800 m at 21:00 UTC on 8 April show the air mass transport within the Arctic haze layer. The trajectories arriving at heights above 4 km suggest that the elevated aerosol layer originated from North America. The optical depth of the aerosol particles above 4 km, however, was estimated to be below 0.02 at 532 nm. Particle backscattering significantly above the background of molecular backscattering was observed up to a height of 9 km on 8–9 April 2002.

The optical parameters of the Arctic haze layer for the period 8 April 2002, 18:23–19:22 UTC in Fig. 7 are characterized in terms of the particle backscatter coefficient, the particle extinction-to-backscatter ratio and the Ångström

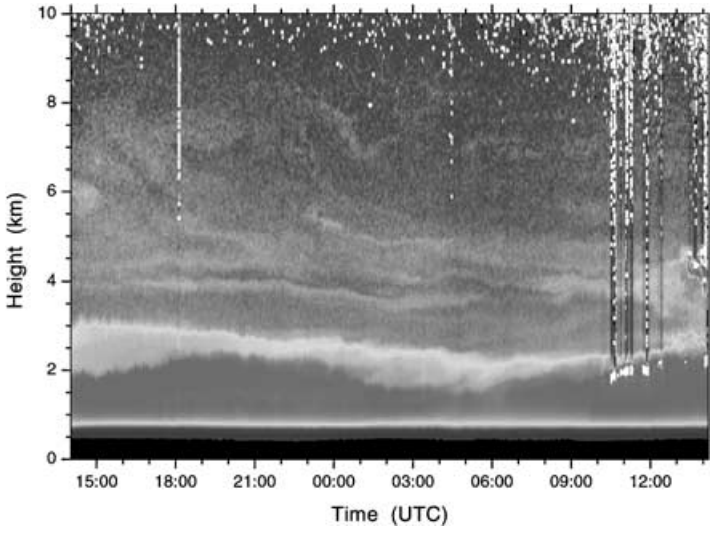

Fig. 5. Range-corrected lidar backscatter signal at 1064 nm measured from 8 April 14:02 UTC (16:02 local time), to 9 April 14:12 UTC. Vertical and temporal resolution is 60 m and 30 s, respectively. The data are reliable at heights above 1 km. The darkest grays indicate the convective boundary layer and aerosol layers above, respectively; light gray indicates weak backscattering, and white shows clouds and signal noise.

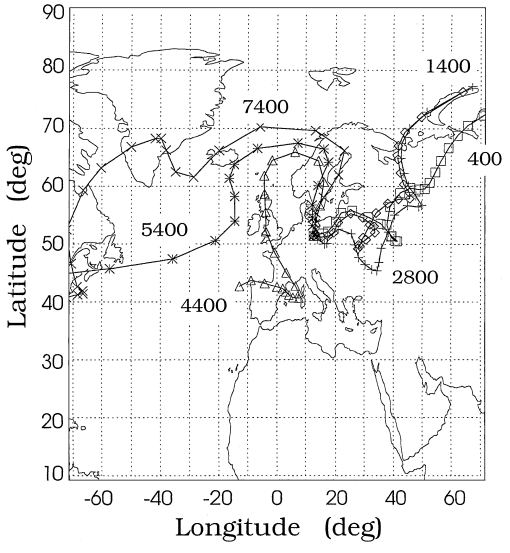

Fig. 6. Ten-day backward trajectories for the arrival heights of 400 m (960 hPa), 1400 m (850 hPa), 2800 m (700 hPa), 4400 m (570 hPa), 5400 m (500 hPa) and 7400 m (370 hPa) above Leipzig. Arrival time is 21:00 UTC on 8 April 2002. The time step between individual symbols is 12 h.

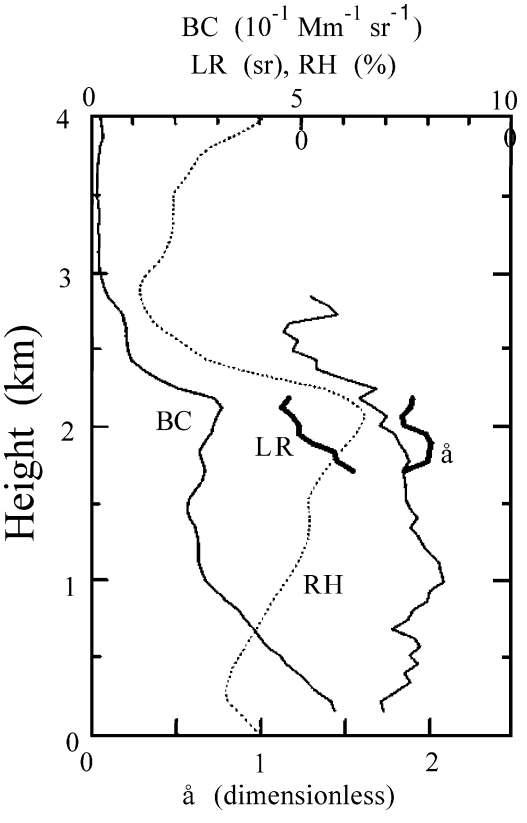

Fig. 7. Lidar observations of the particle backscatter coefficient (BC, 532 nm, thin solid line, top scale), particle lidar ratio (LR, 532 nm, thick solid, top scale), Ångström exponents (AE, from 355/532 nm backscatter, thin solid line, bottom scale) and (AE, from 355/532 nm extinction, thick solid), and relative humidity (RH,%, dotted line, top scale). The measurements were made on 8 April 2002, 1823–1922 UTC (cf. Fig. 5). Lidar ratio and Ångström exponent were only evaluated for the height region between 1.8 and 2.2 km with best lidar data coverage. The radiosonde (RH) was launched at 21:52 UTC.

exponent, *å*, determined from the backscatter coefficients [$å = -\ln(\mathrm{BC355/BC532})/\ln(355/532)$] and from the volume extinction coefficients [$å = -\ln(\mathrm{EC355/EC532})/\ln(355/532)$] at the two wavelengths 355 and 532 nm. The relative humidity (RH) profile of a concurrent radiosonde launched at IfT indicates an almost well mixed boundary layer with RH values from close to 30% at 200 m height to about 65% at 2.2 km height. The extinction coefficient profile at 532 nm shows values of 170–220 M m^{-1} between 1 and 2 km height. These values are typical for air masses arriving from Eastern Europe according to the cluster analysis of trajectories (Mattis et al., 2000a,b). The mean 532-nm extinction coefficient for the Eastern Europe cluster (upper part of the boundary layer, summer half year, April–September) was found to be close to 200 M m^{-1}, and the mean height of the aerosol layer was about 2.5 km. The cluster-mean extinction values for the Eastern Europe cluster is about a factor of two higher than the respective values for westerly, southwesterly and southerly air flows in the respective trajectory clusters. Lidar ratios of 50–60 sr are typical in European pollution aerosols (Ansmann et al., 2001). The lidar ratio at 355 nm was 5% larger than the corresponding value at 532 nm. According to Mie scattering calculations the lidar ratio increases by about 5% for a given particle size distribution of less- or non-absorbing particles when the wavelength is changed from 532 to 355 nm. This increase indicates that the particles were weakly absorbing at both wavelengths.

Ångström exponents were rather high, with values from 1.7 to 2 below 2.2 km height, indicating that particle scattering is dominated by small particles with diameters well below 355 nm (shortest laser wavelength). Data inversion calculations based on the backscatter data at the three laser wavelengths and the extinction data at 355 and 532 nm between 1800 and

2200 m height yield an effective diameter of 0.24 μm, and volume and surface area concentrations of 21 μm^3 cm^{-3} and 540 μm^2 cm^{-3}, respectively. In Table 1 these lidar results are compared to average aerosol characteristics derived for the same period from the ground-based particle size distribution and optical depth measurements at IfT. In case of the sun photometer data, all optical depths measured after 12:00 UTC were averaged. Considering the fact that very different approaches are being compared and their considerable inherent uncertainties, the agreement in derived integral aerosol properties is very good. The fact that similar results of particle surface area, volume and effective radius are obtained at the Earth's surface and at 1800–2000 m height indicate a well-mixed Arctic haze layer. The nearly height-independent Ångström exponent shown in Fig. 7 also indicates that the aerosol characteristics did not change significantly with height within the lowermost troposphere.

3.6. Radiative transfer calculations

The significance of the investigated Arctic aerosol intrusion for the energy balance over Central Europe was investigated with a one-dimensional radiative transfer model. The afternoon of 8 April was chosen for the calculations because sun photometer data and evening lidar data were available (cf. Table 1). As input the following experimental data were employed. Surface volume size distribution, fitted with a single log-normal function type, vertical profile of lidar backscattering coefficients at 532 nm wavelength, with which the surface aerosol volume concentration was extrapolated up to 5 km altitude in the vertical, and meteorological radiosonde data. Doing so yields a calculated optical thickness of 0.42 as compared to the measured value of 0.4–0.44. Spectral irradiances at the top of the atmosphere (TOA) were calculated with and without aerosol particles and integrated over the whole solar spectral range. Two assumed aerosol compositions were investigated: (a) 5% (by volume) soot plus 95% (by volume) ammonium sulfate and (b) pure ammonium sulfate. Model exercises have shown that the choice of specific non-absorbing substance is uncritical for an estimate of the overall optical effects of the aerosol (Wex et al., 2002). No measurements were available for aerosol absorption during the investigated period. However, considering the seasonal variation of absorbing material near Leipzig (Heintzenberg and Bussemer, 2000), a 5% (by volume) soot fraction can be seen as a reasonable assumption.

TOA aerosol forcing for the two assumed aerosol compositions was -23 W m^{-2} (case a) and -38 W m^{-2} (case b), respectively. These values are comparable to the radiative effects measured in the aerosol plumes from North America (Russell et al., 1999) and the Indian subcontinent (Ramanathan et al., 2002). They are considerably higher than corresponding summer values of -4 to -13 W m^{-2} in rather clear air masses of the same region (Wendling et al., 2002).

4. Conclusions

An untypical aerosol situation over Leipzig, Germany in April 2002 was investigated with a comprehensive set of ground-based aerosol volumetric and columnar data, combined with lidar and radiosonde profiles and detailed air mass information. During a contiguous period of 6.5 d on average 25% of the length of 10-d trajectories from Leipzig had been spent north of the Arctic circle before arrival in the planetary boundary layer over Leipzig. For a contiguous period of 2.25 d, the respective value was even 45%. During nine contiguous hours of this period trajectories passed over the greater Moscow region before continuing to Leipzig. An evaluation of aerosol size distributions during these periods showed that frequently number concentrations below about 70 nm in diameter were below long-term average data from 1–15 April 1997–2001 while number, surface and volume concentrations of the particles larger than about 70 nm in diameter were larger than the long-term averages. The lidar profiles showed that the imported aerosol layer was present up to about 3 km height.

With a one-dimensional radiative transfer model solar radiative forcing of the aerosol layer at the top of the atmosphere was estimated for a period with detailed vertical information. Solar particle forcing values between -23 and -38 W m^{-2} were derived, which are comparable to values which have been reported in heavily polluted continental plumes outside the respective source regions. Previous reports have indicated that strong natural aerosol import to Central Europe occurs aloft, coming from the Sahara (e.g. Mattis et al., 2002b). Also, plumes from North America have been observed aloft over Central Europe (e.g. Wandinger et al., 2002). The present report adds weight to these findings, pointing to the need to attribute the three-dimensional aerosol burden over Europe to natural and anthropogenic sources

as well as to aerosol imports from adjacent or distant source regions. In the present case, the transport situation is further complicated by forward trajectories from Central Europe, indicating that some of the observed Arctic haze may have originated in Central Europe before being transported to the European Arctic. From there the haze was re-imported in a modified and augmented form to its initial source region. The investigated aerosol episode shows that chemical weather models are needed that carry a fully interactive aerosol lifecycle model along with the classical meteorology before we can assess and attribute aerosol effects on weather and climate over Europe.

5. Acknowledgements

We gratefully acknowledge the sun photometer data from Lindenberg, Germany kindly provided by the German Weather Service, represented by Dr. Leiterer. This study was partly funded by the German Federal Ministry for Education and Research within the Atmospheric Research Program 2000 (AFO 2000) as part of the project CARLOTTA.

REFERENCES

Ansmann, A., Wagner, F., Althausen, D., Müller, D., Herber, A. and Wandinger, U. 2001. European pollution outbreaks during ACE 2: Lofted aerosol plumes observed with Raman lidar at the Portuguese coast. *J. Geophys. Res*. **106**, 20 725–20 734.

Birmili, W., Stratmann, F., Wiedensohler, A., Covert, D., Russell, L. M. and Berg, O. 1997. Determination of differential mobility analyzer transfer functions using identical instruments in series. *Aerosol Sci. Technol*. **27**, 215–223.

Birmili, W., Stratmann, F. and Wiedensohler, A. 1999. Design of a DMA-based size spectrometer for a large particle size range and stable operation. *J. Aerosol Sci*. **30**, 549–553.

Birmili, W., Wiedensohler, A., Heintzenberg, J. and Lehmann, K. 2001. Atmospheric particle number size distribution in Central Europe: Statistical relations to air masses and meteorology. *J. Geophys. Res*. **106**, 32 005–32 018.

Bösenberg, J., Ansmann, A., Baldasano, J. M., Balis, D., Böckmann, C., Calpini, B., Chaikovsky, A. P., Flamant, P., Hagard, A., Mitev, V., Papayannis, A., Pelon, J., Resendes, D. P., Schneider, J., Spinelli, N., Trickl, T., Vaughan, G., Visconti, G. and Wiegner, M. 2000. EARLINET: A European aerosol research lidar network. In: *Advances in laser remote sensing* (eds. A. Dabas, C. Loth and J. Pelon). Ecole Plytechnique, Palaiseau, France, 155–158.

Covert, D. S. and Heintzenberg, J. 1993. Size distributions and chemical properties of aerosol at Ny-Ålesund, Svalbard. *Atmos. Environ*. **27A**, 2989–2997.

ECMWF 1995. *User guide to ECMWF products 2.1*. Report European Center for Medium Range Weather Forecasting.

Heintzenberg, J. and Larssen, S. 1983. SO_2 and SO_4 in the Arctic: Interpretation of observations at three Norwegian Arctic-subArctic stations. *Tellus* **35B**, 255–265.

Heintzenberg, J., Hansson, H.-C., Ogren, J. A., Covert, D. S. and Blanchet, J.-P. 1986. Physical and chemical properties of Arctic aerosols and clouds. In: *Arctic air pollution* (ed. B. Stonehouse). Cambridge University Press, Cambridge, U.K., 25–35.

Heintzenberg, J. and Bussemer, M. 2000. Development and application of a spectral light absorption photometer for aerosol and hydrosol samples. *J. Aerosol Sci*. **31**, 801–812.

Holben, B. N., Eck, T. F., Slutsker, I., Tanré, D., Buis, J. P., Setzer, A., Vermote, E., Reagan, J. A., Kaufman, Y. J., Nakajima, T., Lavenu, F., Jankowiak, I. and Smirnov, A. 1998. AERONET-A federated instrument network and data archive for aerosol characterization. *Remote. Sens. Environ*. **66**, 1–16.

Mattis, I., Jaenisch, V., Müller, D., Franke, K. and Ansmann, A. 2000. Classification of particle extinction profiles derived within the framework of the German lidar network by the use of cluster analysis of backtrajectories. In: *Advances in laser remote sensing* (ed. A. Dabas, C. Loth and J. Pelon). Ecole Polytechnique, Palaiseau, France, 211–214.

Mattis, I., Ansmann, A., Althausen, D., Jänisch, V., Wandinger, U., Müller, D., Arshinov, Y. F., Bobrovnikov, S. M. and Serikov, I. B. 2002a. Relative humidity profiling in the troposphere with a Raman lidar. *Appl. Opt*. **41**, 6451–6462.

Mattis, I., Ansmann, A., Müller, D., Wandinger, U. and Althausen, D. 2002b. Dual-wavelength Raman lidar observations of the extinction-to-backscatter ratio of Saharan dust. *Geophys. Res. Lett*. **29**, 10.1029/2002GL014721.

Mitchell, J. M. J. 1959. Visual range in the polar regions with particular reference to the Alaskan Arctic. *J. Atmos. Terr. Phys. Spec. Suppl*. **1**, 195–211.

Müller, D., Wandinger, U., Althausen, D. and Fiebig, M. 2001. Comprehensive particle characterization from 3-wavelength Raman-lidar observations: Case study. *Appl. Opt*. **40**, 4863–4869.

Olivier, J. G. J. and Berdowski, J. J. M. 2001. Global emissions sources and sinks. In: *The climate system* (ed. J. Berdowski, R. Guicherit and B. J. Heij). A.A. Balkema Publishers/Swets & Zeitlinger Publishers, Lisse, The Netherlands, 33–78.

Rahn, K. A., Borys, R. D. and Shaw, G. E. 1977. The Asian source of Arctic haze bands. *Nature* **268**, 713–715.

Rahn, K. A. 1982. Elemental tracers for source regions of Arctic pollution aerosol. *Idöjaras* **86**, 1–14.

Ramanathan, V., Crutzen, P. J., Lelieveld, J., Mitra, A. P., Althausen, D. Anderson, J., Andreae, M. O., Cantrell, W.,

Cass, G. R., Chung, C. E., Clarke, A. D., Coakley, J. A., Collins, W. D., Conant, W. C., Dulac, F., Heintzenberg, J., Heymsfield, A. J., Holben, B., Howell, S., Hudson, J., Jayaraman, A., Kiehl, J. T., Krishnamurti, T. N., Lubin, D., MacFarquhar, G., Novakov, T., Ogren, J. A., Podgorny, I. A., Prather, K., Priestley, K., Prospero, J. M., Quinn, P. K., Rajeev, K., Rasch, P., Rupert, S., Sadourny, R., Satheesh, S. K., Shaw, G. E., Sheridan, P. and Valero, F. P. J. 2002. The Indian Ocean Experiment: An integrated analysis of the climate forcing and effects of the great Indo-Asian haze. *J. Geophys. Res*. **106**, 28 371–28 398.

Russell, P. B., Livingston, J. M., Hignett, P., Kinne, S., Wong, J., Chien, A., Durkee, P. and Hobbs, P. V. 1999. Aerosol-induced radiative flux changes off the United States Mid-Atlantic coast: Comparison of values calculated from sunphotometer and in situ data with those measured by airborne pyranometer. *J. Geophys. Res*. **104**, 2289–2307.

Shaw, G. E. 1975. The vertical distribution of tropospheric aerosols at Barrow, Alaska. *Tellus* **27**, 39–49.

Stohl, A., Wotawa, G., Seibert, P. and Kromp-Kolb, H. 1995. Interpolation errors in wind fields as a function of spatial and temporal resolution and their impact on different types of kinematic trajectories. *J. Appl. Meteorol*. **34**, 2149–2165.

Stohl, A., Hittenberger, M. and Wotawa, G. 1998. Validation of the Lagrangian particle dispersion model FLEXPART against large scale tracer experiments. *Atmos. Environ*. **32**, 4245–4264.

Stohl, A. and Seibert, P. 1998. Accuracy of trajectories as determined from the conservation of meteorological tracers. *Q. J. R. Meteorol. Soc*. **125**, 1465–1484.

Stohl, A., Eckhardt, S., Forster, C., James, P. and Spichtinger, N. 2002. On the pathways and timescales of intercontinental air pollution transport. *J. Geophys. Res*. **107**, 10.1029/2001JD001396, 4684, 2002.

Tang, I. N. and Munkelwitz, H. R. 1993. Composition and temperature dependence of the deliquescence properties of hygroscopic aerosols. *Atmos. Environ*. **27A**, 467–473.

Wandinger, U., Müller, D., Böckmann, C., Althausen, D., Matthias, V., Bösenberg, J., Weiß, V., Fiebig, M., Wendisch, M., Stohl, A. and Ansmann, A. 2002. Optical and microphysical characterization of biomass-burning and industrial-pollution aerosols from multiwavelength lidar and aircraft measurements. *J. Geophys. Res*. **107**, 10.1029/2000JD000202.

Wendisch, M., Keil, A., Müller, D., Wandinger, U., Wendling, P., Stifter, A., Petzold, A., Fiebig, M., Wiegner, M., Freudenthaler, V., Armbruster, W., von Hoyningen-Huene, W. and Leiterer, U. 2002. Aerosol–radiation interaction in the cloudless atmosphere during LACE 98. Part 1: Measured and calculated broadband solar and spectral surface insolations. *J. Geophys. Res*. **107**, 10.1029/2000JD000226, 2002.

Wendling, P., Stifter, A., Petzold, A., Fiebig, M., Kiemle, C., Flentje, H., Wendisch, M., Ansmann, A., Armbruster, W. and Hoyningen-Huene von, W. 2002. Aerosol–radiation interaction in the cloudless atmosphere during LACE 98. Part 2: Aerosol induced solar irradiance changes determined from airborne pyranometer measurements and calculations. *J. Geophys. Res*. **107**, 10.1029/2000JD000288, 2002.

Wex, H., Neusüß, C., Wendisch, M., Koziar, C., Keil, A., Ebert, M., Stratmann, F. and Wiedensohler, A. 2002. Particle scattering, backscattering, and absorption coefficients: An in-situ closure and sensitivity study. *J. Geophys. Res*. **107**, 10.1029/2000JD000226, **107**, 10.1029/2000JD000234, 2002.

Wiedensohler, A. 1988. An approximation of the bipolar charge distribution for particles in the submicron size range. *J. Aerosol Sci*. **19**, 387–389.

Wiedensohler, A., Orsini, D., Covert, D. S., Coffmann, D., Cantrell, W., Havlicek, M., Brechtel, F. J., Russell, L. M., Weber, R. J., Gras, J., Hudson, J. G. and Litchy, M. 1997. Intercomparison study of the size-dependent counting efficiency of 26 condensation particle counters. *Aerosol Sci. Technol*. **27**, 224–242.